PEGylation of MnO nanoparticles via catechol–Mn chelation to improving T_1-weighted magnetic resonance imaging application

Haitao Huang,[1] Tao Yue,[2] Yanyun Xu,[3] Ke Xu,[3] Haibo Xu,[1] Shiyuan Liu,[4] Jiahui Yu,[3] Jin Huang[3,5]

[1]Department of Radiology, Union Hospital, Tongji Medical College, Huazhong University of Science and Technology, Wuhan 430022, People's Republic of China
[2]Modern Testing Services Co., Ltd., Shanghai 201108, People's Republic of China
[3]Shanghai Engineering Research Center of Molecular Therapeutics and New Drug Development, School of Chemistry and Molecular Engineering, East China Normal University, Shanghai 200062, People's Republic of China
[4]Department of Diagnostic Imaging, Changzheng Hospital, Shanghai 200003, People's Republic of China
[5]College of Chemistry, Chemical Engineering and Life Science, Wuhan University of Technology, Wuhan 430070, People's Republic of China
Haitao Huang and Tao Yue contributed equally to this work.
Correspondence to: J. Yu (E-mail: jhyu@sist.ecnu.edu.cn) and J. Huang (E-mail: huangjin@iccas.ac.cn)

ABSTRACT: To enhance biocompatibility and physiological stability of hydrophobic MnO nanoparticles as contrast agent of T_1-weighted magnetic resonance imaging (MRI), dopamine-functionalized poly(ethylene glycol) (PEG) was used to coat the surface of about 5 nm MnO nanoparticles. Although hydrophilic coating might decrease longitudinal relaxivity due to inhibiting the intimate contact between manganese of nanoparticle surface and proton in water molecules, higher longitudinal relaxivity was still maintained by manipulating the PEGylation degree of MnO nanoparticles. Moreover, *in vivo* MRI demonstrated considerable signal enhancement in liver and kidney using PEGylated MnO nanoparticles. Interestedly, the PEGylation induced the formation of about 120 nm clusters with high stability in storing and physiological conditions, indicating passive targeting potential to tumor and prolonged circulation in blood. In addition, the cytotoxicity of PEGylated MnO nanoparticles also proved negligible. Consequently, the convenient PEGylation strategy toward MnO nanoparticles could not only realize a good "trade-off" between hydrophilic modification and high longitudinal relaxivity but also contribute additional advantages, such as passive targeting to tumor and long blood circulation, to MRI diagnosis of tumor. © 2015 Wiley Periodicals, Inc. J. Appl. Polym. Sci. **2015**, *132*, 42360.

INTRODUCTION

Early accurate diagnosis of solid tumors is a fundamental prerequisite for effective therapeutic intervention. Magnetic resonance imaging (MRI) is an important method in clinical tumor diagnosis and response evaluation.[1,2] To improve the sensitivity and accuracy of MRI, contrast agents are widely used in clinical practice of MRI diagnosis.[3–5] In this case, the most commonly used contrast agent in MRI is gadolinium chelates;[6,7] however, they suffer stability problem and would release a small amount of free gadolinium ions, which are known to inhibit calcium channels and show considerable toxicity toward liver and kidney.[8–10]

Manganese possesses five unpaired electrons, and the spin of them in manganese perturbs the relaxation of proton in water molecules, which results in an efficient shortening of longitudinal relaxation time, and hence increases the intensity of magnetic resonance signal.[11–13] Furthermore, the toxicity of manganese is much lower than gadolinium, and, meanwhile, it is very interesting that the MnO nanoparticles could provide a rigid crystalline environment that is expected to effectively prevent nanoparticles from releasing free manganese ions.[14] On the other hand, in comparison with iron oxide nanoparticulate as T_2-weighted contrast agents, the MnO nanoparticles could contribute bright field of T_1-weighted MRI, which can be more easily distinguished as they enhance signal instead of reducing it. In T_2-weighted imaging, physiological conditions of bleeding or calcification can be misinterpreted, as both can have a similar effect on the resulting dark signal.[15,16] As a result, the application of the MnO nanoparticles as contrast agent of MRI has

gained considerable attention.[16–19] It is generally recognized that only when the manganese of nanoparticles is intimately close to water molecules, namely, it could directly contact with the proton in water molecules, predominant contrast effect of MnO nanoparticles can be realized.[17,20] Therefore, it is expected to synthesize monodispersed MnO nanoparticles, which size is as small as possible to provide greater specific surface area in comparison with large size particles. In addition, as the as-synthesized MnO nanoparticles are generally hydrophobic, hydrophilic surface modification is essential to render these MnO nanoparticles hydrophilic and biocompatible. However, the "trade-off" between hydrophilic modification and high longitudinal relaxivity should be considered to meet with the request of clinical MRI application because hydrophilic coating might inhibit the direct contact between manganese of nanoparticle surface and proton in water molecules and hence reduce longitudinal relaxivity.

In this work, the MnO nanoparticles with a size of less than 10 nm in a uniform size distribution were first synthesized, and subsequently, the PEGylation was carried out via the conjugation of dopamine-terminated poly(ethylene glycol) (PEG) monomethyl ether with the surface of MnO nanoparticles based on the chelation mechanism between catechol group and manganese. Because there are hydrophilic PEG segments together with hydrophobic MnO nanoparticles and catechol group in one precursor, amphipathy might result in the formation of new structured nano-objects. In this case, the hydrophilic PEG segments might contribute higher stability in aqueous media and even physiological condition; however, the effect of PEGylation degree, by changing the proportion between dopamine-terminated PEG monomethyl ether (mPEG) and MnO nanoparticles, on the longitudinal relaxivity should be investigated to realize a good "trade-off" between hydrophilic modification and good MRI effect. At last, to verify the potential of clinical MRI application for PEGylated MnO nanoparticles, the cytotoxicity and *in vivo* T_1-weighted contrast function were evaluated.

MATERIALS AND METHODS

Materials
Dichloromethane, *n*-hexane, *N*,*N*′-dimethylformamide (DMF), triethylamine (Et$_3$N), acetone, diethyl ether, and thionyl chloride (SOCl$_2$) were purchased from Sinopharm Chemical Reagent, Shanghai, China. DMF was dried with 4 Å molecular sieves and then redistilled before use. Oleic acid, succinic anhydride, and 1-tetradecene were acquired from Aladdin. Manganese chloride, dopamine hydrochloride, and mPEG (M_n: 2000 Da) were obtained from Sigma-Aldrich. Moreover, α-methoxy-amino-PEG (mPEG-NH$_2$) was synthesized according to the previous report.[21]

Cell Line and Culture
Human lung adenocarcinoma cell line (A549) was supplied by the Institute of Biochemistry and Cell Biology, Chinese Academy of Sciences, China. The cells were cultured in RPMI 1640 (Gibco BRL, Paris, France) supplemented with 1% L-glutamine, 10% fetal bovine serum (FBS, HyClone, Logan, UT), streptomycin with a dose of 100 μg mL^{-1}, and penicillin with a dose of 100 U mL^{-1}. The cells were incubated at 37°C under humidified 5% CO$_2$ atmosphere. Finally, cells were splitted by using 0.25% trypsin/EDTA solution when almost confluent.
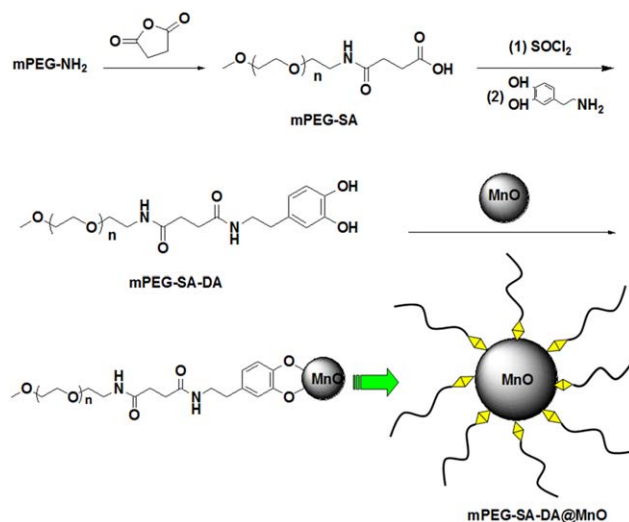

Figure 1. Schematic illustration for the synthesis of mPEG-SA-DA and subsequent coating of mPEG-SA-DA toward MnO nanoparticles. [Color figure can be viewed in the online issue, which is available at wileyonlinelibrary.com.]

Preparation of MnO Nanoparticles
The MnO nanoparticles were prepared by thermal decomposition of manganese oleate.[22,23] First, manganese oleate was prepared according to the following procedure: 3.97 g (20 mmol) of manganese chloride tetrahydrate and 11.30 g (40 mmol) oleic acid were dissolved in 80 mL of methanol. Then, a solution of 1.6 g (40 mmol) sodium hydroxide in 80 mL of methanol was added dropwise into the stirred Mn−/oleic acid solution over a period of 1 h. In this step, the initially clear colorless mixture turned pink, and a deep red oily substance precipitated. After being stirred for another hour, the solvent was discarded, and the product was washed with water, ethanol, and acetone. Thereafter, the oily residue was dissolved in hexane and dried over MgSO$_4$. After evaporating the solvent, the product was dried *in vacuo* (1 × 10^{-2} mbar) at 100–150°C for 2 h to produce a deep red waxy solid.

Subsequently, 1.86 g (3 mmol) of the manganese oleate was dissolved in 10 g of 1-tetradecene and degassed at 70°C *in vacuo* (1 × 10^{-2} mbar) for 2 h. Then, the reaction mixture was treated with a definitive temperature program as follows: initially, the solution was rapidly heated to 200°C with ∼ 5°C min^{-1}. For the further course of the reaction, the heating rate was fixed at 1.5°C min^{-1}, and the temperature was held at reflux (245°C) for 30 min. At last, the as-synthesized nanoparticles were washed three times according to the following procedure: dispersing in hexane and precipitating with ethanol, and finally collected by centrifugation. The washed MnO nanoparticles were redispersed in hexane for storage.

Synthesis of Dopamine-Terminated Poly(ethylene glycol) Monomethyl Ether Linked with Succinic Anhydride
Figure 1 depicts the synthesis process of dopamine-terminated mPEG linked with succinic anhydride (mPEG-SA-DA). The process included the following two steps: first, to a dried DMF solution (100 mL) of mPEG-NH$_2$ (3.80 g, 2 mmol), a solution

Table I. Theoretical Maximum Coating Densities of mPEG-SA-DA on the Nanoparticle Surface and Corresponding Longitudinal Relaxivity (r_1) for the mPEG-SA-DA@MnO Nano-Objects with Various Feeding Ratios of mPEG-SA-DA versus MnO Nanoparticles

Sample no.	Feeding ratio of mPEG-SA-DA versus MnO (mg mg^{-1})	Theoretical maximum coating density of mPEG-SA-DA (mmol m^{-2})	r_1 (mM^{-1} S^{-1})
mPEG-SA-DA@MnO(1)	100/20	17.22	5.98
mPEG-SA-DA@MnO(2)	80/20	14.79	6.15
mPEG-SA-DA@MnO(3)	60/20	13.33	6.29
mPEG-SA-DA@MnO(4)	40/20	7.35	7.83
mPEG-SA-DA@MnO(5)	20/20	6.51	16.14

of succinic anhydride (0.24 g, 2.4 mmol) and Et$_3$N (0.33 mL, 2.4 mmol) in 20 mL dried DMF was added dropwise under nitrogen atmosphere, and then the reaction would proceed for 24 h at room temperature. Methanesulfonic acid (0.16 mL, 2.4 mmol) was added to the solution to convert the Et$_3$N salt form of mPEG-SA to its acid form. After filtration, the resulting succinic acid-functionalized mPEG (mPEG-SA) was isolated by precipitation in cold ether and vacuum-dried to give a yield of 85%. The structure of mPEG-SA was verified by ^{1}H nuclear magnetic resonance (^{1}H NMR; 400 MHz, CDCl$_3$) and depicted in detail as follows: δ (ppm) of 3.38–3.63 (m, $-CH_2CH_2O-$), 2.65 (t, $-COCH_2CH_2COOH$), 2.55 (t, $-COCH_2CH_2COOH$).

Second, mPEG-SA (2.00 g, 1 mmol) was reacted with SOCl$_2$ (40 mL) at 85°C for 4 h under nitrogen atmosphere and then evaporated out the unreacted SOCl$_2$ under reduced pressure. Subsequently, the mixture was dissolved in 40 mL of dried CH$_2$Cl$_2$, and a solution of 3-hydroxytyramine hydrochloride (227 mg, 1.2 mmol) and Et$_3$N (0.17 mL, 1.2 mmol) in 10 mL dried CH$_2$Cl$_2$ was added dropwise into the above solution under nitrogen atmosphere. At last, the resulting mPEG-SA-DA was isolated by precipitation in ether twice and then dialyzed (molecular weight cutoff size: 1000 Da) against deionized water for 3 days at room temperature. The yield was 66%. The structure of mPEG-SA was verified by ^{1}H NMR (400 MHz, D$_2$O) and depicted in detail as follows: δ (ppm) of 6.51–6.75 (m, phenolic ring), 3.39–3.64 (m, $-CH_2CH_2O-$), 2.56–2.63 (t, $-COCH_2CH_2C-$).

Fabrication of mPEG-SA-DA@MnO Nano-Objects

As shown in Figure 1, by changing the feeding ratio of mPEG-SA-DA versus MnO nanoparticles, the mPEG-SA-DA@MnO nano-objects with various theoretical maximum densities of mPEG-SA-DA on the nanoparticle surface were prepared (the @ means enclosed). Briefly, 100, 80, 60, 40, and 20 mg of mPEG-SA-DA in CHCl$_3$ were mixed with 5 mL n-hexane containing 20 mg of the MnO nanoparticles. After the mixture was stirred for 3 h at room temperature, the solvent was evaporated to produce the mPEG-SA-DA@MnO nano-objects. Subsequently, the product was redispersed in water and then dialyzed (molecular weight cutoff size: 14,000 Da) against deionized water for 3 days at room temperature. Accordingly, the as-prepared nano-objects were sampled as mPEG-SA-DA@MnO(1), mPEG-SA-DA@MnO(2), mPEG-SA-DA@MnO(3), mPEG-SA-DA@MnO(4), and mPEG-SA-DA@MnO(5) in the descending order of feeding

mPEG-SA-DA amount, and the composition and character of every sample are summarized in Table I. Herein, the theoretical maximum coating densities of mPEG-SA-DA on the nanoparticle surface according to the size of MnO nanoparticles were calculated according to the literature.[11]

For cell viability assays and in vivo T_1-weighted MRI, the lyophilized mPEG-SA-DA@MnO nano-objects were sterilized under UV for 45–60 min and then redispersed in corresponding sterilized media.

Characterization

The chemical structures of mPEG-SA-DA and mPEG-SA were verified by ^{1}H NMR on a Bruker Avarice^{TM} 400 NMR spectrometer. At the same time, Fourier transform infrared (FTIR) spectra were recorded on Nicolet Nexus 670 spectrometer. The samples were pressed into pellets with KBr.

The particle size and size distribution of the mPEG-SA-DA@MnO nano-objects were measured by dynamic light scattering (DLS; Zeta-Sizer Nano ZS, Malvern Instruments, UK). Meanwhile, for transmission electron microscopy (TEM) observation, 10 μL of sample solution with a concentration of 0.01 mg mL^{-1} was carefully dropped onto copper grids and then dried at 50°C for 35 min before being photographed on JEM-100C II microscope (LIBRA 120, Carl Zeiss, Germany).

Stability Evaluation of mPEG-SA-DA@MnO Nano-Objects

To evaluate the stability under storing and physiological conditions, mPEG-SA-DA@MnO nano-objects were redispersed in PBS (pH 7.4) and cell culture medium in which there was 10% FBS to simulate physiological condition and then conditioned at 4°C and at 37°C for 30 days, respectively. For two systems, the changes of hydrodynamic diameter were traced by DLS. Triple measurements were carried out, and the number–weighted mean size was taken.

Cell Viability Assays of mPEG-SA-DA@MnO Nano-Objects

In vitro cytotoxicity of the mPEG-SA-DA@MnO nano-objects to inhibiting cells growth was evaluated by determining the viability of A549 cell line via MTT method. Briefly, the cells were seeded in 96-well plates with 50 μL fresh culture medium, and then another 50 μL culture medium which contains various concentrations of mPEG-SA-DA@MnO nano-objects was added into the 96-well plates. After incubation for 24 h, 10 μL of MTT (0.5 mg mL^{-1}) was added to the culture medium solution for further 4-h incubation. Then, the culture medium was
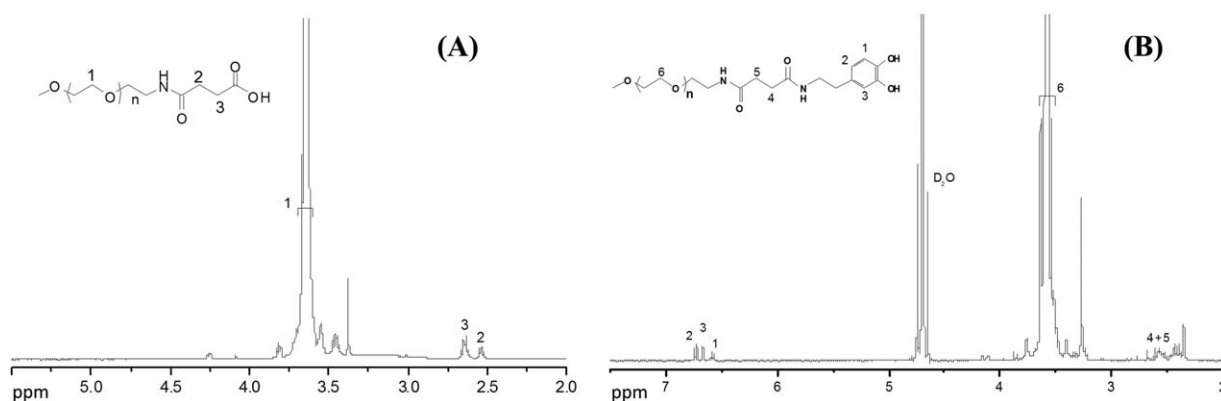
Figure 2. ^{1}H NMR spectra of mPEG-SA (A) in CDCl$_3$ and mPEG-SA-DA (B) in D$_2$O.

removed, and the insoluble formazan-containing crystals were dissolved by adding 100 μL of DMSO to each well. The optical density (OD) was measured at 570 nm using an automatic BIO-TEK microplate reader (Powerwave XS, USA), and the cell viability was calculated from the following equation:

$$\text{Cell viability } (\%) = \frac{\text{OD}_{\text{sample}}}{\text{OD}_{\text{control}}} \times 100\%, \qquad (1)$$

where OD$_{\text{sample}}$ represents an OD value from a well treated with the solution containing mPEG-SA-DA@MnO nano-objects, and OD$_{\text{control}}$ comes from a well treated with only PBS. Each experiment was carried out in sextuplet, and the mean and corresponding standard deviations (mean ± SD) were shown as the results.

Longitudinal Relaxivity of mPEG-SA-DA@MnO Nano-Objects
The longitudinal relaxivity (r_1) of mPEG-SA-DA@MnO nano-objects was measured at 37°C using a Siemens Tim 3T MRI scanner. The mPEG-SA-DA@MnO nano-objects were redispersed in water at the manganese concentrations in the range of 0.0625–1 mM. For MRI measurements, 1.5 mL solutions were filled into each of the test tubes to determine the longitudinal relaxation time (T_1). The measurement at each manganese concentration was done in triplicate, and the average value of T_1 was taken. The longitudinal relaxivity (r_1) was

determined by a linear fit of the inverse longitudinal relaxation time ($1/T_1$) as a function of the manganese concentrations.

In Vivo T$_1$-Weighted MRI of mPEG-SA-DA@MnO Nano-Objects
A 4-week male ICR mouse with a weight of 20–25 g was used to evaluate the MRI enhancement effect of mPEG-SA-DA@MnO nano-objects as T_1 contrast agent. The mouse ($n = 6$) was anesthetized by 100 μL pelltobarbitalum natricum solution with a concentration of 1.0%. Measurements for each mouse were carried out on a Siemens Tim 3T MRI scanner before and after injecting mPEG-SA-DA@MnO nano-objects into a mouse tail vein at the Mn dose of 0.5 mg per kg (the weight of mouse). The imaging parameters were depicted as follows: repetition time = 280 ms; echo time = 15 ms; field of view = 90 mm; matrix size = 256 × 114; slice thickness = 2.0 mm; number of acquisition = 9.

Statistical Data Analysis
Statistical data analysis was performed using the Student's t-test.

RESULTS AND DISCUSSION

Structures of mPEG-SA-DA and Intermediate Product
As illustrated in Figure 1, succinic acid-functionalized mPEG (mPEG-SA) was synthesized by the reaction between mPEG-NH$_2$ and succinic anhydride. The chemical shifts of mPEG-SA
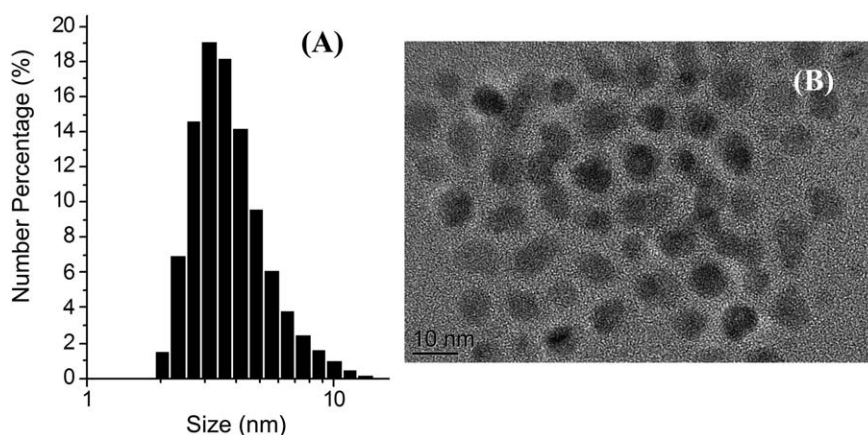

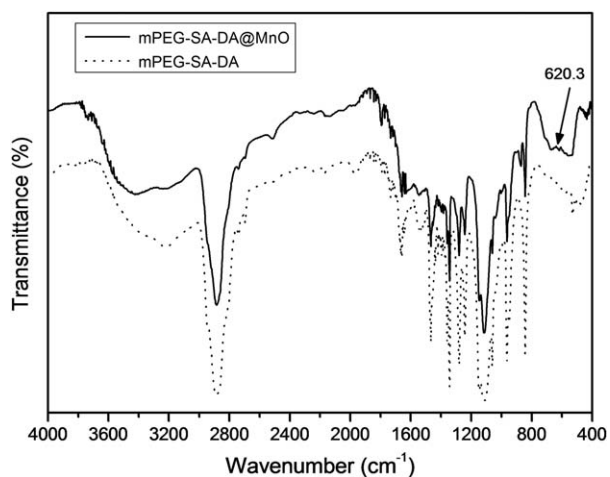**Figure 3.** Size distribution curve (A) and TEM image (B) of MnO nanoparticles.

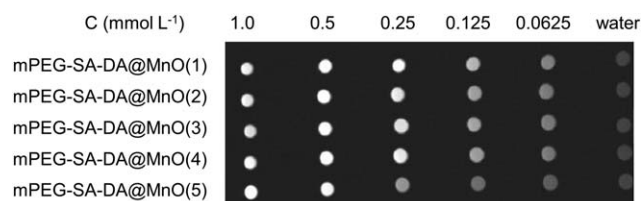**Figure 4.** FTIR spectra of mPEG-SA-DA (A) and mPEG-SA-DA@MnO nano-objects (B).

Figure 5. Phantom images functioned as the Mn concentrations in the suspensions of mPEG-SA-DA@MnO nano-objects with various feeding ratio of mPEG-SA-DA vesrus MnO nanoparticles.

are shown in Figure 2(A). The typical signals of PEG could be observed at 3.38–3.63 ppm (Peak 1). The peaks located at 2.55 ppm (Peak 2) and 2.65 ppm (Peak 3) are assigned to succinate moiety. Then, the amino group of dopamine was coupled with carboxyl group of mPEG-SA to produce dopamine-terminated mPEG-SA (mPEG-SA-DA). The structure of mPEG-SA-DA was verified by ^{1}H NMR, and the spectrum is shown in Figure 2(B). The typical signals of PEG could also be observed at 3.39–3.64

ppm (Peak 6). Furthermore, the peaks located at 2.56–2.63 ppm (Peaks 4 and 5) were assigned to succinate, and the peaks located at 6.51–6.75 ppm (Peaks 1–3) belong to the phenolic ring of dopamine moiety.

Size and Morphology of MnO Nanoparticles

As it is well known, the small size as possible would contribute the Gd_2O_3 nanoparticles to better T_1-weighted contrast function because their high ratio of surface versus volume (P) corresponded to higher longitudinal relaxivity (r_1).[24] As a result, the as-prepared MnO nanoparticles in this work were also expected to be in the size of several nanometers. Figure 3 shows the size distribution curve and TEM image of the as-prepared MnO nanoparticles. The size distribution curve measured by DLS [Figure 3(A)] showed that the average diameter of the MnO nanoparticles was about 5 nm. Furthermore, the MnO nanoparticles were observed as approximate spherical shape by the TEM image in Figure 3(B) and showed nearly monodispersed state. In addition, the diameters of nanoparticles were determined in the range of 4–6 nm from the TEM image, which was well consistent with the DLS result.

Fabrication of mPEG-SA-DA@MnO Nano-Objects

For most as-prepared MnO nanoparticles, the organic solvents used as dispersing media inhibit their practical MRI application because of their instability in aqueous media including *in vivo* environment. Furthermore, the hydrophobic surface of MnO nanoparticles might result in bad biocompatibility. As a result, hydrophilic surface modification is essential for the MRI application *in vivo* of MnO nanoparticles to realize long-term blood circulation and match other physiological factors. In this case, the PEGylation is well known as a good and facile method. As the metal—O bonding can be formed between transition metal and catechol, the dopamine-containing mPEG-SA-DA can result in multiple catechol binding onto the surface of MnO nanoparticles via the Mn—O bonding.[25] As shown in the FTIR spectra in Figure 4, in comparison with the FTIR spectrum of mPEG-SA-DA, the new adsorption bands at 620.3 cm^{-1} assigned to
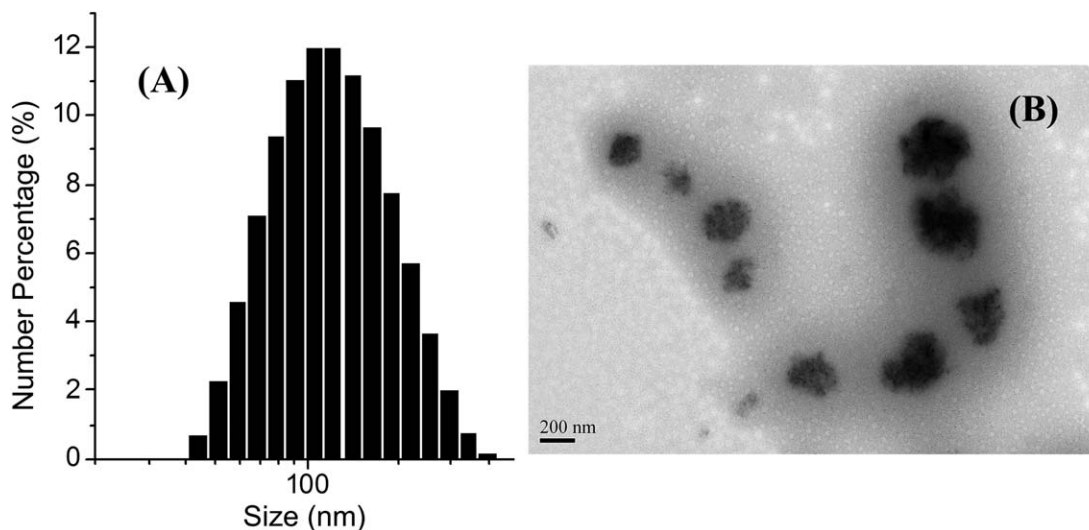

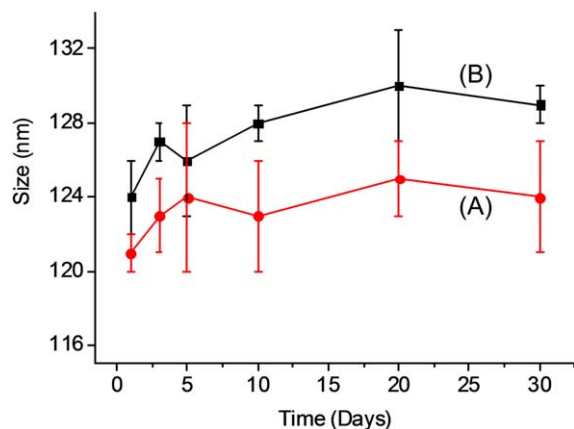**Figure 6.** Size distribution curve (A) and TEM image (B) of mPEG-SA-DA@MnO(5) nano-objects.

Figure 7. Average size functioned as the time of mPEG-SA-DA@MnO(5) nano-objects in PBS (pH 7.4) at 4°C (A) and cell culture medium (B) at 37°C (mean ± SD, $n = 3$). [Color figure can be viewed in the online issue, which is available at wileyonlinelibrary.com.]

the Mn—O bonding confirmed the PEGylation of MnO nanoparticles.

Effects of Surface PEGylation Degree on Longitudinal Relaxivity

As the T_1-weighted MRI of MnO nanoparticles as contrast agent depends on proximity effect, surface PEGylation might hinder the intimate contact between the manganese of the nanoparticle surface and the proton in water molecules and thus inhibit longitudinal relaxivity (r_1) and contrast effect in MRI. In this work, it is a key issue to optimize surface PEGylation degree for the trade-off of high longitudinal relaxivity and

enough hydrophilicity. As shown in Table I, when the theoretical maximum coating density of mPEG-SA-DA was higher than 7.35 mmol m^{-2}, the longitudinal relaxivity was still kept at a level of 6–7 mM^{-1} S^{-1}. However, with a slight decrease of theoretical maximum coating density as 6.51 mmol m^{-2}, the longitudinal relaxivity significantly increased up to 16.14 mM^{-1} S^{-1}. As expected, higher longitudinal relaxivity gave predominant contrast signal. For T_1-weighted MRI, the enhancing contrast effect is shown as brighter field. Figure 5 depicts phantom images functioned as the Mn concentrations in the suspensions of mPEG-SA-DA@MnO nano-objects with various theoretical maximum coating densities of mPEG-SA-DA. Obviously, the mPEG-SA-DA@MnO(5) with the lowest theoretical maximum coating density of 6.51 mmol m^{-2} showed stronger contrast signal, and especially the enhancing contrast effect was predominant at lower Mn concentration.

Size and Morphology of mPEG-SA-DA@MnO Nano-Objects

Based on the above research concerning the effect of surface PEGylation degree on longitudinal relaxivity and *in vitro* enhanced contrast effect, the mPEG-SA-DA@MnO(5) with the lowest theoretical maximum coating density and higher longitudinal relaxivity was selected for further characterization and profound evaluation. Figure 6 shows the size distribution curve and TEM image of mPEG-SA-DA@MnO(5). In the mPEG-SA-DA@MnO nano-objects, amphipathy, which was derived from hydrophilic PEG segments and hydrophobic catechol-chelated MnO nanoparticles, might result in the formation of new structured objects. As shown in the size distribution curve measured by DLS, the hydrodynamic diameters of mPEG-SA-DA@MnO(5) obviously increased, and the average value was located at about 120 nm [Figure 6(A)]. At the same time, the TEM image revealed
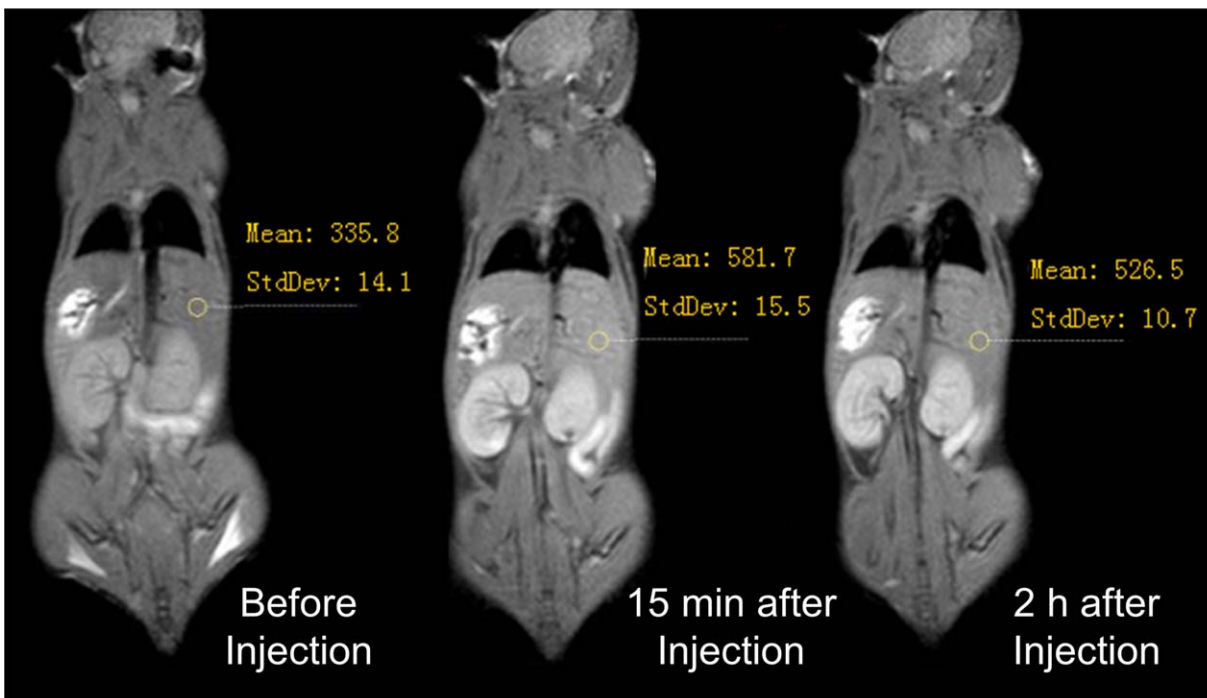

Figure 8. T_1-weighted MRI photographs of the mouse observed before injection and at 15 min and 2 h after injecting mPEG-SA-DA@MnO(5) nano-objects. [Color figure can be viewed in the online issue, which is available at wileyonlinelibrary.com.]
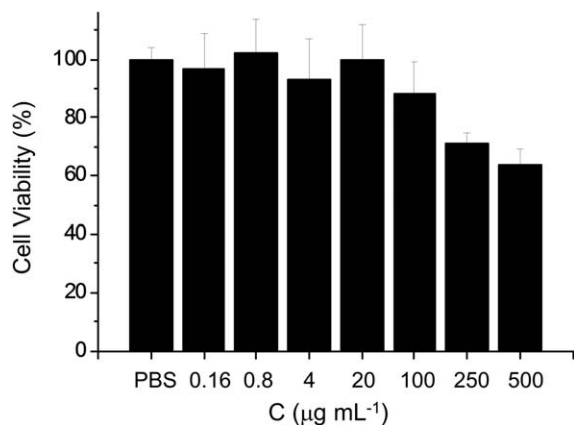
Figure 9. Dependence of cell viability on the Mn concentrations of mPEG-SA-DA@MnO(5) nano-objects against A549 cell line for 24 h (mean ± SD, $n = 6$, $P < 0.05$).

that the mPEG-SA-DA@MnO(5) was a greater spherical nano-object [Figure 6(B)]. Interestingly, such newly formed spherical nano-objects with the average size of about 120 nm and the hydrophilic PEG surface might be endowed with passive targeting potential to tumor tissue and prolonged blood circulation. In other words, the surface PEGylation strategy inhibited the *in vivo* precipitation and easy-to-clearing of unmodified MnO nanoparticles because of their hydrophobic nature and small size of about 5 nm. Furthermore, the converge of many MnO nanoparticles in newly formed of about 120 nm nano-objects might produce better contrast effect due to higher manganese density concentrated in one nanoscaled scope.

Stability of mPEG-SA-DA@MnO Nano-Objects

In theory, surface PEGylation can contribute to high stability of nanoparticles in aqueous media. To verify the storing and *in vivo* stability, the mPEG-SA-DA@MnO(5) was dispersed in PBS (pH 7.4) and cell culture medium containing 10% FBS, which simulated the storing and physiological conditions, respectively, and then conditioned at 4 and 37°C for 30 days. In this period, the DLS was used to trace the change in size. Figure 7 depicts the average sizes of mPEG-SA-DA@MnO(5) functioned as the conditioning time. As expected, when the time prolonged until 30 days, there was almost no change in the size of mPEG-SA-DA@MnO(5). It indicated that the formed nano-objects in the mPEG-SA-DA@MnO(5) system with the modification of the least mPEG-SA-DA amount were very stable in storing and physiological conditions.

In Vivo T_1-Weighted MRI of mPEG-SA-DA@MnO Nano-Objects

To evaluate clinical application potential, *in vivo* MRI study of mPEG-SA-DA@MnO(5) was carried out. Figure 8 shows the T_1-weighted MRI photographs of mouse observed before injection and at 15 min and 2 h after injecting mPEG-SA-DA@MnO(5). It demonstrated that the significant increase of brightness occurred in liver and kidney, indicating considerable accumulation of the mPEG-SA-DA@MnO nano-objects in these two tissues after injection. In comparison with the T_1-weighted liver images before injection and at 15 min after injection, the observed signal intensity enhanced from 335.8 to 581.7. Furthermore, the signal intensity in the T_1-weighted liver image could

still remain 526.5 until 2 h after injection, which was ascribed to long blood circulation period. Such good long-term contrast effect might meet with the request in practical MRI application.

In Vitro Cytotoxicity of mPEG-SA-DA@MnO Nano-Objects

The *in vivo* safety is the primary prerequisite for the mPEG-SA-DA@MnO nano-objects in MRI application, namely, at least acceptable cytotoxicity and even nontoxicity. The *in vitro* cell viability assay against A549 cell line verified the negligible cytotoxicity of mPEG-SA-DA@MnO(5). Figure 9 depicts the representative concentration–growth inhibition bars of the mPEG-SA-DA@MnO(5) toward A549 cell. With an increase in the concentration of mPEG-SA-DA@MnO(5), the cell viability first kept the level of almost no cytotoxicity as about or close to 100% and obviously decreased when the concentration was higher than 250 µg mL^{-1}. The dose-dependent manner for the inhibition toward cell growth provided the preliminary proof of the applicable dose for the mPEG-SA-DA@MnO(5). Even though the concentration of the mPEG-SA-DA@MnO(5) reached 500 µg mL^{-1}, the cytotoxicity was still acceptable by MRI application.

CONCLUSIONS

In this work, the as-prepared MnO nanoparticles with an average size of about 5 nm were PEGylated by dopamine-terminated mPEG (mPEG-SA-DA) to form about 120 nm nano-objects of mPEG-SA-DA@MnO. It was verified that the theoretical maximum coating density of mPEG-SA-DA as 6.51 mmol m^{-2} could realize enough hydrophilicity and higher longitudinal relaxivity of 16.14 mM^{-1} S^{-1}, which corresponded to better contrast effect in MRI. Moreover, in comparison with unmodified MnO nanoparticles, the mPEG-SA-DA@MnO nano-objects showed high stability under storing and physiological conditions. Furthermore, for mPEG-SA-DA@MnO nano-objects, a good and continuous contrast effect until 2 h might meet with the requirement of practical MRI application while negligible cytotoxicity confirmed the safety *in vivo*. Altogether, the facile PEGylation strategy toward MnO nanoparticles gained trade-off between enough hydrophilicity and high longitudinal relaxivity and hence developed a novel T_1-weighted MRI contrast agent.

REFERENCES

1. Brown, M. A.; Semelka, R. C., Eds. MRI: Basic Principles and Applications, 4th ed.; Wiley-Blackwell: Hoboken, **2010**.

2. Sun, Y.; Liu, Q.; Peng, J.; Feng, W.; Zhang, Y.; Yang, P.; Li, F. *Biomaterials* **2013**, *34*, 2289.

3. Rohrer, M.; Bauer, H.; Mintorovitch, J.; Requardt, M.; Weinmann, H. *J. Invest. Radiol.* **2005**, *40*, 715.

4. Caravan, P.; Ellison, J. J.; McMurry, T. J.; Lauffer, R. B. *Chem. Rev.* **1999**, *99*, 2293.

5. Zabow, G.; Dodd, S.; Moreland, J.; Koretsky, A. *Nature* **2008**, *453*, 1058.

6. Hu, F.; Zhao, Y. S. *Nanoscale* **2012**, *4*, 6235.

7. Chen, F.; Bu, W.; Zhang, S.; Liu, X.; Liu, J.; Xing, H.; Xiao, Q.; Zhou, L.; Peng, W.; Wang, L.; Shi, J. *Adv. Funct. Mater.* **2011**, *21*, 4285.

8. Penfield, J. G.; Reilly, R. F. *Nat. Clin. Pract. Nephrol.* **2007**, *3*, 654.

9. Broome, D. R. *Eur. J. Radiol.* **2008**, *66*, 230.

10. Marckmann, P.; Skov, L.; Rossen, K.; Dupont, A.; Damholt, M. B.; Heaf, J. G.; Thomsen, H. S. *J. Am. Soc. Nephrol.* **2006**, *17*, 2359.

11. Na, H. B.; Lee, J. H.; An, K. J.; Park, Y. I. *Angew. Chem. Int. Ed. Engl.* **2007**, *46*, 5397.

12. Im, G. H.; Kim, S. M.; Lee, D.-G.; Lee, W. J.; Lee, J. H.; Lee, I. S. *Biomaterials* **2013**, *34*, 2069.

13. Bennewitz, M. F.; Lobo, T. L.; Nkansah, M. K.; Ulas, G.; Brudvig, G. W.; Shapiro, E. M. *ACS Nano* **2011**, *5*, 3438.

14. Shao, Y.; Tian, X.; Hu, W.; Zhang, Y.; Liu, H.; He, H.; Shen, Y.; Xie, F.; Li, L. *Biomaterials* **2012**, *33*, 6438.

15. Hyeon, T.; Na, H. B. *J. Mater. Chem.* **2009**, *19*, 6267.

16. Gallo, J.; Alam, I. S.; Lavdas, I.; Wylezinska-Arridge, M.; Aboagye, E. O.; Long, N. J. *J. Mater. Chem. B* **2014**, *2*, 868.

17. Park, M.; Lee, N.; Choi, S. H.; An, K.; Yu, S.-H.; Kim, J. H.; Kwon, S.-H.; Kim, D.; Kim, H.; Baek, S.-I.; Ahn, T.-Y.; Park, O. K.; Son, J. S.; Sung, Y.-E.; Kim, Y.-W.; Wang, Z.; Pinna, N.; Hyeon, T. *Chem. Mater.* **2011**, *23*, 3318.

18. Lee, Y.-C.; Chen, D.-Y.; Dodd, S. J.; Bouraoud, N.; Koretsky, A. P.; Krishnan, K. M. *Biomaterials* **2012**, *33*, 3560.

19. Schladt, T. D.; Schneider, K.; Shukoor, M. I.; Natalio, F.; Bauer, H.; Tahir, M. N.; Weber, S.; Schreiber, L. M.; Schröder, H. C.; Müller, W. E. G.; Tremel, W. *J. Mater. Chem.* **2010**, *20*, 8297.

20. Fang, J.; Chandrasekharan, P.; Liu, X.-L.; Yang, Y.; Lv, Y.-B.; Yang, C.-T.; Ding, J. *Biomaterials* **2014**, *35*, 1636.

21. Zalipsky, S.; Gilon, C.; Zilkha, A. *Eur. Polym. J.* **1983**, *19*, 1177.

22. Zhong, X.; Xie, R.; Sun, L.; Lieberwirth, I.; Knoll, W. *J. Phys. Chem. B* **2006**, *110*, 2.

23. Schladt, T. D.; Graf, T.; Tremel, W. *Chem. Mater.* **2009**, *21*, 3183.

24. Park, J. Y.; Baek, M. J.; Choi, E. S.; Woo, S.; Kim, J. H.; Kim, T. J.; Jung, J. C.; Chae, K. S.; Chang, Y.; Lee, G. H. *ACS Nano* **2009**, *3*, 3663.

25. Ling, D.; Park, W.; Park, Y. I.; Lee, N.; Li, F.; Song, C.; Yang, S.-G.; Choi, S. H.; Na, K.; Hyeon, T. *Angew. Chem. Int. Ed. Engl.* **2011**, *50*, 11360.